

Pyrolysis of Date Stones Using Natural Activated Kaolin as a Catalyst – Optimization of Variables and Identification of Bio-Oil

Ahmed S. Ibrahim¹, Abdelrahman B. Fadhil^{1*}

¹ Department of Chemistry, College of Science, Mosul University, Majmoaa Street, 41002, Mosul, Iraq

* Corresponding author's e-mail: abdelrahmanbasil@uomosul.edu.iq

ABSTRACT

This research examines the catalytic performance of the catalyst developed from natural kaolin clay as a cheap catalyst for the thermal pyrolysis of date stones (DS). Firstly, the natural kaolin clay was acid-treated, followed by thermal activation at 600 °C for 2h to obtain the activated kaolin catalyst (AKC). Several techniques, like BET surface area, pore volume distribution, XRD, FESEM, and EDX, were utilized to identify the AKC. The BET surface area of the AKC was 119.49 m²/g, while its mean pore diameter amounted to 7.13 nm, indicating its mesoporosity. The catalytic activity of the AKC was examined via the thermal pyrolysis of DS. Effect of pyrolysis temperature (400–500 °C), catalyst loading (2.5–10.0 wt.%), pyrolysis period (30–120 min), and particle size of DS (0.25, 0.297, 0.4, 0.595, and 0.841 mm) on the pyrolysis products yield was investigated. The highest yield of pyrolytic liquid was produced at 425 °C for 1h using 2.5 wt.% of the AKC and 0.40 mm particle size of the feed. At these conditions, the pyrolytic liquid yield amounted to 60.64%. The analysis of the bio-oil (BO) fraction stripped from the pyrolytic liquid was achieved by FTIR spectroscopy, ¹H NMR spectroscopy, and GC-MS analysis, which indicated that the BO fraction was mainly composed of hydrocarbons and oxygenated hydrocarbons. Results from the GC-MS analysis exhibited that hydrocarbons (48.28%), oxygenates (41.42%), aromatics (10.44%), and nitrogenates (2.13%) were the main components of the BO. Alkenes and n-alkanes were the main constituents of the hydrocarbon part of the BO, while acids were the main component of oxygenates. Non-catalytic thermal cracking of DS at the optimal conditions exhibited a lower pyrolytic liquid yield than the catalytic process. Finally, the fuel properties of the BO produced via catalytic pyrolysis of DS were superior to those measured for that produced by the thermal pyrolysis process.

Keywords: date stones; activated kaolin catalyst; catalytic pyrolysis; bio-oil; identification of BO.

INTRODUCTION

Recent years have witnessed a rise in energy demand because of the more considerable rise in energy consumption. Conventional fundamental energy sources, namely fossil energy sources, couldn't satisfy the world's energy needs (Pan et al., 2021). Moreover, the environmental contamination results from these sources must be noticed. Consequently, searching for new energy sources is imperative (Wang et al., 2021). Among the possible alternative to fossil fuel sources are sustainable energy sources. Biomass (BM), one of these sources, is the most encouraging as it is globally recognized as a renewable and carbon-neutral fuel resource with low SO_x and NO_x emissions (Tursi, 2019). Furthermore, using the

proper technology, biomass can be immediately turned into various forms of energy (solid, gas, and liquid) (Paenpong and Pattiya, 2016). The BM is a complicated blend of hemicellulose, cellulose, lignin, and a trace of other organics, including extractives. Various sources of BM, like fruit seeds (Fadhil and Kareem, 2021), de-oiled cakes (Rajpoot et al., 2022), non-edible seeds (Al-Layla et al., 2021), bagasse (Li et al., 2022), sawdust (Agnihotri and Mondal, 2023), and other forms of BM, were implemented in producing various types of fuel (liquid, gas, and solid). Date stones (DS) are among the bio-wastes employed for producing biofuel because they are abundant and affordable, particularly in Mediterranean nations. Iraq is an essential date supplier worldwide, with more than 21,000,000 date trees, with an

annual production of almost 400,000 tons of date fruit (Ahmed and Theydan, 2015; Younis et al., 2022) The DS are waste materials that account for around 14% of the total mass of the fruit. Beyond the manufacturing of palm syrup, the DS is discarded. As such, eliminating such solid waste is of the essence, as its collection might harm the environment (Ahmed and Theydan, 2015; Younis et al., 2022). Pyrolysis is a thermochemical conversion process that can potentially treat many types of solid wastes besides producing new products. The pyrolysis process involves exposing the solid waste to temperatures ranging from 400 to 800 °C in a deficient atmosphere of oxygen (Silvestre et al., 2020). Heating the solid substrate in an inert environment promotes the thermolysis of the solid waste macromolecules. Thus, liquid products (pyrolytic oil), char (pyrolytic char) and non-condensable gases are produced (Silvestre et al., 2020; Mishra and Mohanty, 2020).

The pyrolytic liquid produced by BM thermal pyrolysis is usually called bio-oil (BO), bio-fuel, or bio-crude. It can be considered a cleaner substitute for fossil fuels since they contribute almost zero CO₂ emissions. It comprises a complicated mixture of oxygenates, saturated and unsaturated hydrocarbons besides the oxygenated compounds (Toro-Trochez et al., 2022; Mekhilef et al., 2012). BO includes essential compounds that could be employed in various applications, including medicinal, cosmetics, agricultural, and industrial products. The O-containing compounds, such as water, acids, aldehydes, and ketones, are the most compounds found in BO (Mariscal et al., 2016; Wang et al., 2022). The BO can't be directly employed as a fuel in automotive engines as they own several drawbacks, including its content of multiple O-compounds, which diminished its quality and made it more viscose with a lower calorific value. Also, the presence of these compound in BO decrease its stability and provoke its corrosion features. Consequently, it is necessary to reduce the level of oxygenated compounds before using them as fuel (Rowhani and Rainey, 2016).

The catalytic pyrolysis (CP) was proposed to lessen the oxygen content in the BO. However, few works were established on the catalytic pyrolysis of DS. In this regard, (Aljeradat et al., 2022) studied the thermal pyrolysis of date kernels using natural Jordanian Tripoli as a low-cost catalyst. (Arabiourrutia et al., 2022). explored catalytic thermal pyrolysis of DS between 450 and 500 °C over HZSM-5

and dolomite as catalysts,(Hai et al., 2022). inspected thermokinetics of the in-situ pyrolysis of DS utilizing layered double hydroxide-based catalysts. Lastly, (Hou et al., 2023). they have explored thermal and catalytic pyrolysis of DS in Py-GC/MS equipment. For the catalytic pyrolysis, HZSM-5 zeolite was employed for this purpose. As mentioned above, direct thermal pyrolysis of BM will result in the formation of products with low quality due to their content of high molecular weight fractions. As such, catalytic pyrolysis was proposed as a potential means to improve the liquid oil yield and quality besides lessening the time and temperature required for thermal pyrolysis (Hou et al., 2023). The most frequent catalysts employed upon thermal pyrolysis solid wastes include zeolite (Arabiourrutia et al., 2022), microporous and acidic mesopores (Saidi et al., 2016), base catalysts (Saidi et al., 2016), and noble transition metals (Saidi et al., 2017), and metal oxide (Saidi et al., 2017). Additionally, transition-metal-supported catalysts have recently gained considerable concern as a catalyst for this purpose (Saidi et al., 2016; Saidi et al., 2017). However, those catalysts are easily deactivated besides being expensive. Thus, low-cost catalysts, such as kaolin, were employed in this respect. Kaolin belongs to the group of layered silicate minerals and is naturally occurring clay. It is composed of a two-layered 1:1 structure that consists of (SiO₄) tetrahedral and (AlO₆) octahedral; the layers are connected by relatively stable hydrogen bonds (Luo et al., 2020).

As far as we know, the catalytic thermal destruction of any BM feed using activated kaolin catalyst (AKC) as a low-cost catalyst has not been announced in the literature. Additionally, employing the AK as an effective catalyst in the thermal cracking of the DS, which is generated with massive amounts as a byproduct of the dates industry to produce an upgraded liquid oil compared to the pyrolysis oil produced via the thermal pyrolysis process with optimizing the experimental conditions affecting the quality and yield of the produced liquid oil, has not been touched to the best of the author knowledge. This issue attracted us to accomplish this research work.

The DS was thermally cracked using acid-activated kaolin clay as a cheap catalyst in this context. The raw kaolin clay was acid treated and thermally activated to be utilized later in the pyrolysis of DS. The thermal decomposition of DS using the AKC was performed by optimizing the working conditions that affect the production of

the maximum liquid yield of oil. The typical BO from DS was identified by GC-MS spectroscopy and ^1H NMR spectroscopy. The FTIR spectroscopy was utilized to specify functional groups in the liquid fuel besides assessing fuel properties of the obtained liquid fuel.

MATERIALS AND METHODS

Materials

The raw materials, namely DS employed in this study, were stripped from the locally produced date fruit. The catalyst was synthesized from the kaolin clay from natural deposits in Dohok City, north of Iraq.

Preparation and analysis of DS

The DS was washed with water, oven-dried at 105 °C for a day, pulverized, and then sieved to obtain homogenous particles (0.40 mm). The DS powder was then subjected to multiple analysis procedures. A Vario EL CUBE, Germany, CHNSO elemental analyzer was employed in determining the elemental analysis of the DS. The ASTM D121 standard approach was adopted to examine the proximate analysis (ash %, moisture %, volatile materials %, and fixed carbon %). Lastly, the thermal degradation tendency of the DS was investigated using the SDT-Q600 TA Simultaneous TGA/DSC, USA, thermal analyzer at a heating rate of 10 °C/min under a stream of dry air and N_2 gas between 28 and 600 °C.

Synthesis of the AKC

The raw kaolin clay was first rinsed with water to eliminate impurities adsorbed on its surface, followed by drying at 105 °C for a day. The dried clay was ground and sieved to obtain particles of 0.149 mm in size. The kaolin clay was mixed with a solution of 10% HCl. The mixture was then refluxed with stirring at 300 rpm for 2h. Afterwards, the acid-treated clay was repeatedly rinsed with distilled water until obtaining neutral water. After drying at 105 °C for 10h, it was thermally activated at 600 °C for 2h to obtain activated kaolin clay (AKC) (Altamer et al., 2022).

Identification of the AKC

The as-prepared catalyst was identified by multiple techniques before its use in thermal

pyrolysis experiments. The catalyst crystallinity was identified by a high-resolution x-ray diffractometer system (Malvern Panalytical X-ray diffraction, UK) with $\text{Cu } \alpha$ radiation (λ) of 0.154 nm at 40 kV and 20 mA in 2θ range of 10° to 90°. A surface area analyzer (BELSORP MINI II, Japan) was employed in determining the total surface area mean pore volume of the catalyst based on the N_2 adsorption/desorption isotherms at 77 K. BET method was followed in calculating the total surface area of the AK. In addition to the elemental analysis of the synthesized catalyst, the morphological features were examined by Field-Emission Scanning Electron Microscope attached to an energy-dispersive X-ray analyzer (Tescan Mira 3 LMU FESEM-EDX, France, 2018).

Pyrolysis experiment using the AKC

The catalytic thermal pyrolysis trials of DS were carried out employing a semi-batch cylindrical reactor made of stainless steel with a length of 30 cm, 4 cm internal diameter, and 5 cm external internal diameter. Thermal pyrolysis was connected with a condensation system to condense the volatile vapors collected in a collector immersed in a cold bath (dry ice+ acetone). The desired temperature was adjusted by a PID controller linked to the furnace. The catalytic thermal cracking experiments of DS were accomplished at numerous feed-to-catalytic ratios in the same reactor. The catalyst was mixed with DS particles at 2.5 wt.%, 5.0 wt.%, 7.5 wt.%, and 10.0 wt.%. Before the thermal pyrolysis experiment, the reactor was flushed for 20 min with N_2 to expel air and other unwanted impurities. When the reaction was ended, the reactor was left to cool down to room temperature, and the solid residue was stripped from the reactor and weighed. Each trial was repeated twice, and the outcome was recorded as the mean \pm SD. The yield of liquid, biochar (BC), and non-condensable gases was calculated using the following equations (Mishra and Mohanty, 2019; Fadhil and Kareem, 2021):

$$\begin{aligned} \text{Yield of liquid (\%)} &= \\ &= \frac{\text{Weight of the liquids produced (g)}}{\text{Total weight of WT or DS utilized (g)}} \times 100 \end{aligned} \quad (1)$$

$$\begin{aligned} \text{Yield of BC (\%)} &= \\ &= \frac{\text{Weight of BC produced (g)}}{\text{Total weight of WT or DS utilized (g)}} \times 100 \end{aligned} \quad (2)$$

$$\begin{aligned} \text{Yield of gases (\%)} &= \\ &= 100 - [\% \text{ liquid yield} + \% \text{ BC yield}] \end{aligned} \quad (3)$$

In addition to optimizing the amount of catalyst required for maximum conversion of DS into liquid fuel, other factors, like pyrolysis temperature (400–600 °C), period of pyrolysis (30–150 min), and the feed particle size (0.841, 0.595, 0.40, 0.297, and 0.25 mm) were optimized as well.

Analytical methods of the BO

The pyrolytic liquid produced after the catalytic and catalytic thermal decomposition of the DS was fractionated into two phases. The upper was the bio-oil (BO) phase, while the lower was the aqueous phase. The BO phase was submitted to various analysis methods, including Fourier Transform Infrared (FTIR) spectrophotometer (JASCO V-630, USA), which was employed to inspect the functional groups in the liquid oil fraction. The chemical components of the BO fraction were figured out on a Gas chromatography-mass spectrometry (GC-MS, Agilent 8860-5977B) employing helium as the carrier gas at 1 mL min⁻¹ a flow rate. The injector temperature and injection volume were respectively fixed at 280 °C and 1 µL. The oven program was initiated at 60 °C (1 min), elevated to 200 °C at 12 °C min⁻¹ rate of heating, and then the temperature was raised to 280 °C at a heating rate of 5 °C min⁻¹ where it was preserved for 4 min (Fadhil and Kareem, 2021). The liquid fuel samples from the were identified by ¹H NMR spectroscopy utilizing a 400-MHz spectrometer from Bruker Biospin GmbH. As a solvent, CDCl₃ was used, while Tetra Methyl Silane (TMS) served as the internal standard. Finally, the density (ASTM D1217-209), kinematic viscosity (ASTM D445), flash point (ASTM D93), pour point (D2500), and acidity of the obtained liquid fuel were all measured. All measurements were completed using standardized protocols established by the ASTM.

RESULTS AND DISCUSSION

Characterization of the AKC

The AKC was utilized as a low-cost catalyst in the pyrolysis of DS. Thus, it was first identified by numerous techniques to assess its textural and morphological features. Fig. 1a shows the N₂-adsorption-desorption isotherm of the AKC besides the pore volume distribution. The N₂ adsorption isotherm was type III as per the IUPAC

classification. Also, Fig. 1a showed that adsorption of the N₂ increased at the relative pressure region ($P/P_0 < 0.1$), specifying that few micropores are found in the AKC (Hou et al., 2023). Besides, the relative pressure region ($P/P_0 = 0.2–0.9$) disclosed the creation of abundant micropores and mesopores in the AKC. Moreover, the presence of the H3 hysteresis loop at the relative pressure regions ($P/P_0 = 0.4–1.0$) confirmed the presence of mesopores in the AKC (Panda et al., 2010). Additionally, a sharp uptake at ($P/P_0 > 0.9$) was seen in the N₂-adsorption-desorption curves, suggesting the existence of large mesopores or even macropores in the structure of the AKC. The presence of such pores is essential for mass transfer during catalytic reactions (Hou et al., 2023). The BET surface area of the AKC amounted to 119.49 m²/g, while the mean pore volume of the AKC was 7.13 nm, implying its mesoporous.

The BJH surface area, which measures the mesopores surface area, amounted to 90.58 m²/g. As such, the mesopores surface area participation in the as-synthesized catalyst was 75.53%, confirming that mesopores are the superior pores in the porous structure of the AKC. The morphological features of the AKC surface were examined by FESEM, and its image is demonstrated in Fig. 1b. It is evident from the FESEM image of the AKC that its surface was asymmetrical, dissimilar, and contained multiple pores and cavities with various shapes and sizes. The presence of such pores is helpful for the mass transfer during catalytic reactions of the DS structure, which coincides with the N₂-adsorption isotherm. The EDX technique explored the elemental analysis of the AKC. As shown in Fig. 1b, the EDX map results exhibited that Si, O, Fe, Al, Mg, and K were the main elements forming the AKC. The reddish color of the AKC is attributed to its content of Fe. The crystalline structure of the AKC was inspected by XRD analysis, which is depicted in Fig. 1c. The XRD pattern of the AKC showed numerous diffraction peaks. Also, as per these peaks, kaolinite (Al₂Si₂O₅(OH)₄) and quartz were the main phases of the AKC. The diffraction peaks relating to quartz were those observed at $2\theta = 20.80^\circ, 26.59^\circ, 50.03^\circ, 59.91^\circ, \text{ and } 68.27^\circ$. The XRD phases relating to kaolinite were those located at $2\theta = 12.1^\circ, 14.15^\circ, 17.25^\circ, 24.0^\circ, 27.89^\circ, 30.35^\circ, 33.29^\circ, 35.61^\circ, 39.53^\circ, 42.44^\circ, 45.81^\circ, 54.31^\circ, 64.01^\circ, \text{ and } 75.46^\circ$. The XRD phases observed in the AKC were compatible with those established elsewhere (Hou et al., 2023).

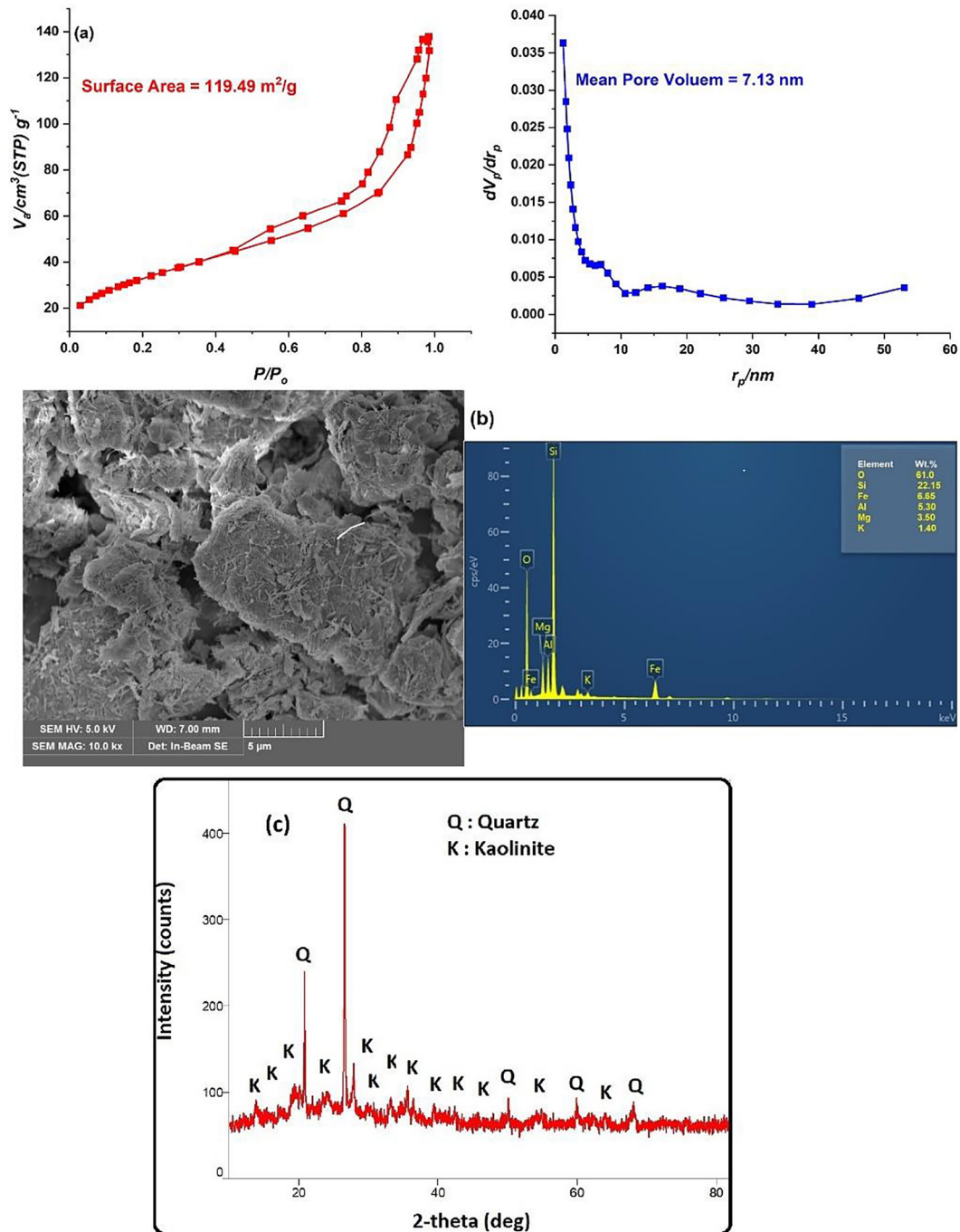


Figure 1. (a) N_2 adsorption-desorption isotherms, (b) XRD pattern, and (c) FESEM image and EDX map of the AKC

Table 1. The ultimate and proximate analyses of DS compared to other seeds

Element (%)	DS	<i>Pongamia pinnata</i> seed (Pan et al., 2021)	<i>Cascabela Thevetia</i> seed (Wang et al., 2021)
C	48.50	43.80	46.08
H	7.42	6.40	7.20
N	0.65	3.90	6.43
O (by difference)	43.43	41.50	40.29
HHV (MJ/kg)	17.65		19.25
Moisture	1.55	7.0	5.10
Fixed carbon	14.20	10.30	16.82
Volatiles	82.0	78.10	73.81
Ash	2.25	4.60	4.20

Analysis of the raw DS

The proximate and ultimate analyses afford the feasibility of BM as a pyrolysis precursor. The detailed proximate and ultimate analyses outcomes of the DS are offered in Table 1 on a dry basis, along with ultimate and proximate analyses results of other non-edible seeds.

The outcomes derived from the elemental analysis of DS disclosed that the results were comparable to that of other seeds (Doshi et al., 2014; Sut et al., 2016). The C and H contents in the DS were above those established for *Pongamia pinnata* seeds (Doshi et al., 2014) and *Cascabela Thevetia* seeds (Sut et al., 2016). Also, the DS possessed a lower N- content than other seeds (Table 1), suggesting that its emission of NO_x will be less upon pyrolysis (Mishra and Mohanty, 2019). The proximate analysis results disclosed that the moisture content of the DS was below 10.0 %. According to (Ahmad et al., 2017), BM feed with lower moisture content is recommended as a feedstock for combustion and pyrolysis. The higher volatile and lower ash contents in the DS than other seeds confirmed its high ignition efficiency as fuel. Besides, it was reported that the heating value of the feed is inversely proportional to its ash content (Mishra and Mohanty, 2018). The fixed carbon content (14.20 %) was also comparable to other seeds in the literature. The contents of the volatile combustible matter s, besides the fixed carbon of the feed, directly participate in the heating value of any fuel (Mishra and Mohanty, 2018). The TGA curve for the DS is demonstrated in Figure 2,

which shows that as the temperature increases, the weight loss increases as well. The first stage of thermal decomposition occurs between 60 °C and 200 °C, indicating the loss of moisture and physically adsorbed H_2O molecules (Mohan et al., 2023). At a temperature range of 200 °C – 450 °C, the maximum thermal decomposition occurred, signifying the evolution of the volatile compounds. The volatiles produced at this stage of thermal decomposition are the main sources for producing the pyrolytic liquid, which could be employed as a liquid fuel or a source for chemicals. Also, this stage is considered the active pyrolysis zone where the breaking of the weaker chemical bonds, intermolecular association, and side aliphatic chains occurs (Mohan et al., 2023). The third stage of thermal cracking occurred between 450 °C and 600 °C. This stage is usually slow and nearly steady, leaving behind a solid residue (biochar) (Mohan et al., 2023).

Catalytic pyrolysis experiments

The catalytic thermal cracking of DS was accomplished by optimizing conditions affecting the products yield, particularly the liquid yield, to find out the ideal conditions that will produce the maximum amount of the liquid fuel. The catalytic thermal pyrolysis of the DS was performed at multiple temperatures ranged from 400 °C to 500 °C with an increment of 25 °C per experiment. At the same time, the catalyst loading, time, particle size, and heating rate were fixed, as presented in the legend of Fig. 3a. It is clear from this figure that the liquid yield increased when

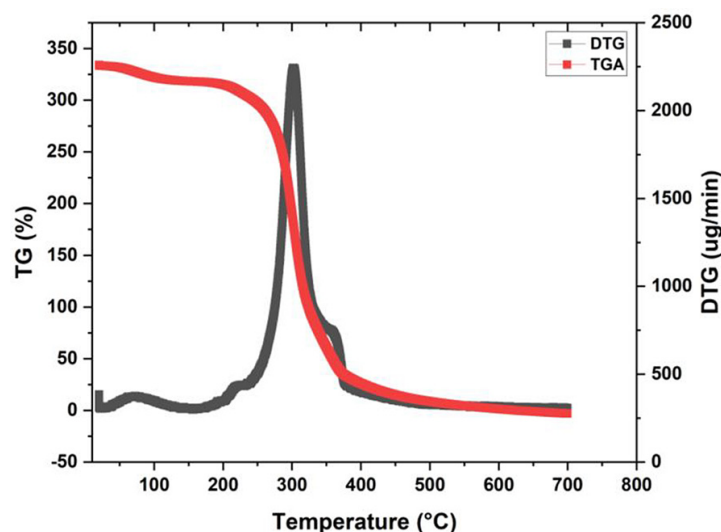


Figure 2. TGA-DTG curves of the DS

the pyrolysis temperature raised from 400 °C to 425 °C, and then a decline in the liquid yield was observed. The maximum yield of the pyrolytic liquid was produced at 425 °C. At 400 °C, the thermal cracking of the DS was incomplete, resulting in a lower yield of the liquid fraction (Fadhil and Kareem, 2021). At the typical temperature of pyrolysis (425 °C), the heat and mass transfer between the DS particles happened extensively, leading to the formation of maximum hot volatiles (Mishra and Mohanty, 2020). Pyrolysis temperatures above 425 °C lessened the liquid yield because of the quick endothermic decomposition of the DS, which converts condensable volatiles into non-condensable vapors, resulting in diminish in the pyrolytic oil yield. A pyrolysis temperature of 425 °C was below that observed upon thermal decomposition of the DS, which was 500 °C (Fadhil et al., 2017). It was evident from Fig. 3a that the BC decreased while the yield of the gaseous products increased with the rising

pyrolysis temperature. These consequences belong to the secondary thermal cracking reactions of the feed in addition to the produced BC into non-condensable vapors (Fadhil, 2021). The obtained findings were compatible with those established for the catalytic pyrolysis of Manilkara zapota seeds using ZSM-5 as a catalyst (Mishra and Mohanty, 2020).

The catalysts-to-feed ratio (C/F) is the critical process variable, which can considerably change the pyrolytic products yield and properties of the produced pyrolytic oil. Thus, multiple ratios of the AKC (2.5–10.0 wt.%) were tried upon catalytic pyrolysis of the DS. These experiments were accomplished using the conditions presented in the legend of Fig. 3b. It was observed that the pyrolytic oil yield diminished as the (C/F) ratio increased. The highest yield of the pyrolytic oil was produced at 2.5 wt.% of the catalyst. From the chemistry point of view, the presence of the catalyst will provide more active sites for the process.

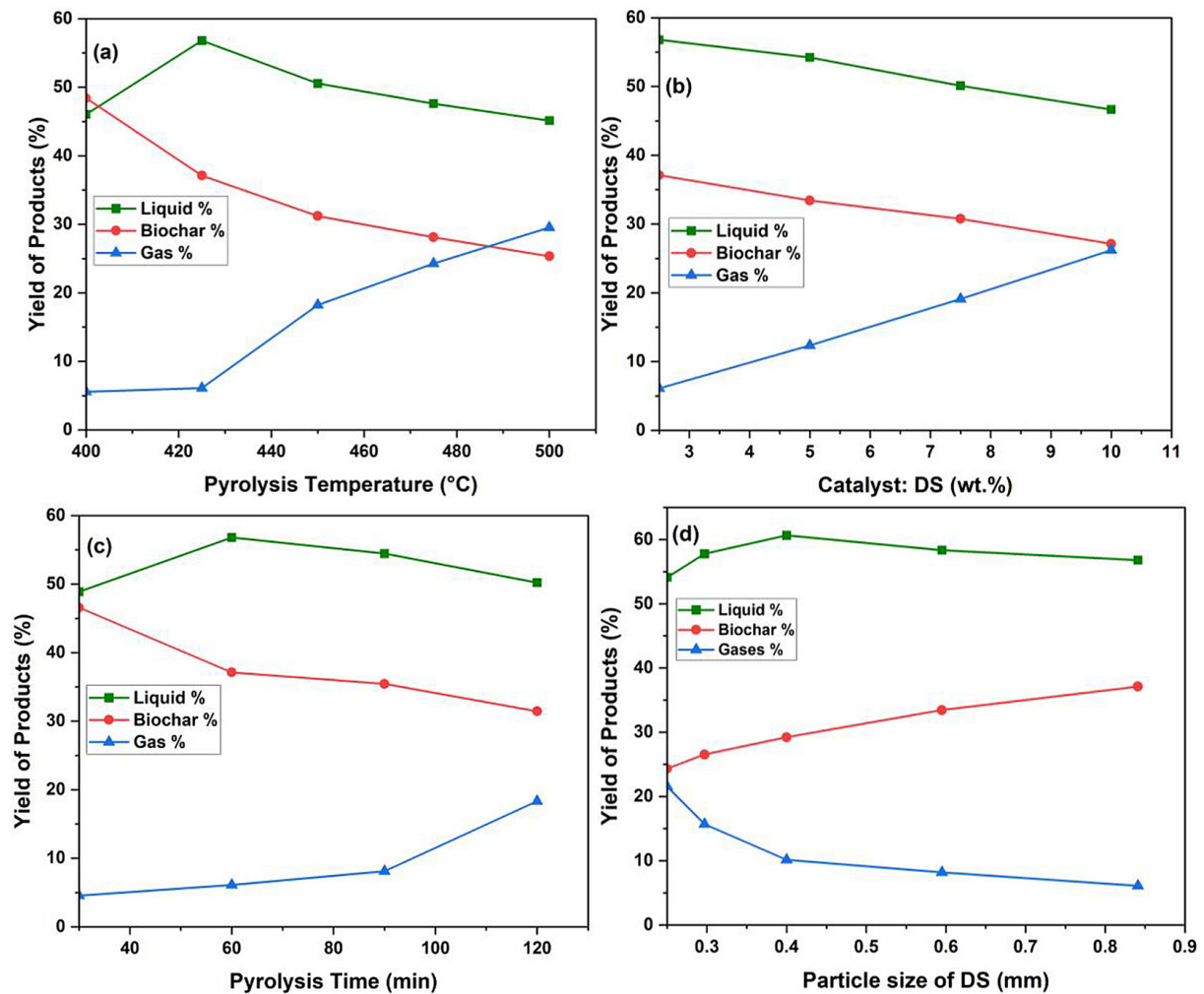


Figure 3. (a) Effect of temperature, (b) catalyst loading, (c) time, and (d) particle size on the pyrolysis products yields

These will accelerate the decarboxylation and decarbonylation reactions of the BM feed into volatile materials, forming more pyrolytic liquid (Mishra and Mohanty, 2020; Fadhil, 2021). Nevertheless, the excessive amounts of the catalyst diminished yields of both the pyrolytic liquid and the BC. At the same time, it increased the yield of the gaseous products. This consequence could be ascribed to the fact that using higher quantities of the AKC is associated with the availability of a large number of catalytic active sites, which will boost the secondary cracking of feed, BC, and volatiles into non-condensable gases (Fadhil, 2021). Also, when the amount of the catalyst exceeds the optimal, the decarboxylation and thermal cracking reactions of the pyrolytic oil and heavy matter will be more severe, causing a decline in the BO and BC yield and a rise in the gaseous product yield (Aljeradat et al., 2022). Our findings aligned with the announcement for the catalytic thermal cracking of Manilkara zapota seeds and the DS using various catalysts (Mishra and Mohanty, 2020; Aljeradat et al., 2022).

Another essential variable that must be optimized upon the thermal destruction process is the time the feed spends inside the reactor as a consequence of its impact on the product's yields. This variable controls the contact period between the feed particles and the heating area. As such, the best time for the process should be chosen (Fadhil et al., 2017). On this account, the catalytic pyrolysis of the DS achieved various durations in the range of 30–150 minutes while keeping other variables fixed, as given in the legend of Fig. 3c. The result presented in this figure demonstrated that short periods of pyrolysis resulted in a low liquid yield as a result of imperfect decomposition of the feed into the desired products due to insufficient heat transfer from the pyrolysis zone to the feed particles via conduction (Fadhil and Kareem, 2021). The liquid yield increased when the pyrolysis time was extended from 30 to 60 min, while durations beyond 60 min declined the liquid yield. In addition, when the pyrolysis duration exceeds the optimal period, the endothermic nature of the pyrolysis process increases the likelihood of the conversion of condensable gases into non-condensable gases, which reduces the BO yield (Fadhil and Kareem, 2021; Fadhil et al., 2017). In contrast, the BC yield decreased while the gaseous product output increased with extending the pyrolysis period. This phenomenon results from the secondary thermal decomposition reactions that cause the additional

gasification of acquired condensable vapors and char into non-condensable vapors. Consequently, BO and BC yields decreased, whereas the gaseous products yield increased (Altamer et al., 2021). Similar results were obtained from the pyrolysis of mixed date kernels and olive stones (Fadhil and Kareem, 2021), Mandarin (*Citrus reticulata*) seeds (Fadhil et al., 2017), wild mustard seeds (Altamer et al., 2021), and milk thistle (*Silybum marianum* L.) seeds (Uzun et al., 2007).

The particle size of the BM feed is another crucial variable that affects the distribution and output of pyrolysis products. The particle size of the feed employed for thermal cracking is substantially related to the heat and mass transfer rates. Moreover, changing the particle size of the feed affects the heating rate of the BM feedstock, thereby altering the pyrolysis action of the BM feedstock (Uzun et al., 2007). Consequently, the effect of DS particle size on the pyrolysis product yield was investigated. Pyrolysis of the DS was accomplished using particles of multiple sizes (0.25, 0.297, 0.40, 0.595, and 0.841 mm) with keeping other parameters constant, as presented in the legend of Fig. 3(d), their typical values. The BO yield decreased as the DS particle size increased, as shown in Fig. 3d. The results suggested that neither the heat and mass transmission accompanying the decomposition mechanism nor the uniform heating of BM particles improved when employing larger particle sizes (Mishra and Mohanty, 2018). As depicted in Fig. 3d, the BC yield decreased as the DS particle size decreased. At the same time, the gaseous products increased due to the smaller particle size's ability to gasify the raw BM quicker under controlled pyrolysis conditions due to the rapid mass and heat transfer (Mishra and Mohanty, 2018). This is generally consistent with the pyrolysis treatment outcomes for wild mustard seeds (Altamer et al., 2021), milk thistle seeds (Al-Layla et al., 2021), and blue-green algae colonies (Hu et al., 2013).

Based on the results, the highest liquid yield was produced at 425 °C for 60 min using 2.5 wt.% of AKC and 0.40 mm particle size. To recognize the potential of the as-prepared catalyst, thermal pyrolysis of the DS applying the conditions above were employed, and the outcomes are presented in Figure 4, which showed that the liquid yield produced via the catalytic pyrolysis was considerably above that produced without catalyst. This finding could be attributed to the fact that the presence of a catalyst will accelerate the thermal destruction of high molecular weight

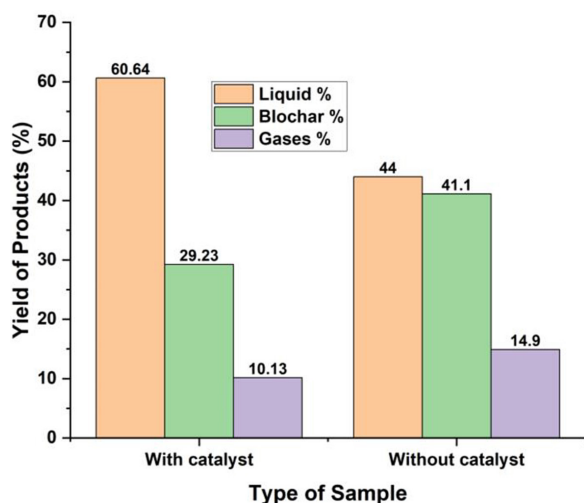


Figure 4. Pyrolysis products yield of DS via catalytic and thermal pyrolysis

components of the DS at a lower temperature compared to the thermal pyrolysis process, which needs a higher temperature to reach maximum conversion of the DS into liquid oil. On the other hand, the BC yield was higher in the thermal pyrolysis process than that of the catalytic pyrolysis due to the presence of a catalyst, which enhances the thermal decomposition of the formed BC into volatile components.

Analysis of BO produced by thermal and catalytic pyrolysis of DS

The pyrolytic liquid produced by the catalytic thermal pyrolysis of DS at the optimal pyrolysis conditions was separated into two fractions by a separating funnel. The upper fraction was the oil (BO), while the lower fraction was the aqueous phase. This is due to that using pyrolytic liquid directly as a fuel is not recommended because of its high content of water, which causes many problems, including corrosion of engines or burners, besides lessening its heating value. Also, the presence of water in the pyrolytic liquid affects its authentic properties, like density, viscosity, pour point, flash point, and acidity. So, it is recommended to separate and identify the bio-oil fraction, which content of O is lower than that of the pyrolytic liquid besides its features, which qualify it as an alternative to diesel fuel or fuel for boilers without problems. For comparison, the oil phase from the thermal decomposition of DS was separated in the same manner. Various Techniques were employed in analyzing both BO samples, as follows:

GC-MS spectrometry

The BO samples originating from the catalytic and thermal pyrolysis of DS were analyzed by Gas Chromatography-Mass Spectrometry to recognize the unknown constituents present in the pyrolytic oil. The mass spectra originating from both samples were matched with the National Institute of Standards and Technology (NIST) library. Compounds derived from the GC-MS for both BO samples are tabulated in Tables 2 and 3.

Following the results presented in these tables, it was found that the BO is a multi-blend of highly oxygenated compounds with large-sized molecules, including almost oxygenated organics, such as carboxylic acids, esters, phenols, alcohol, ethers, aldehydes, ketones and amide compound. Also, it was conveyed that over 300 diverse types of organic compounds were identified in the pyrolytic oil as a consequence of its assorted complex composition (Mishra and Mohanty, 2019), and these different groups separated into six main classes, like mono-aromatics, heterocyclic, aliphatic, oxygenates, polyaromatics, and nitrogenates. Analysis of the BO produced by the catalytic thermal cracking of DS by GC-MS analysis demonstrated that it was mainly composed of hydrocarbons (48.28%), oxygenates (41.28%), aromatics (10.44%), and nitrogenates (2.13%). The hydrocarbon part included 31.21% alkenes 14.64% n-alkanes, and 2.4% iso-alkanes. On the other hand, the oxygenates fraction was chiefly composed of acids (37.79%), and esters (3.38%). The same compounds were also found in the BO produced by thermal pyrolysis of DS, but with different percentages. Table 4 compares the percentage of compounds present in the BO produced via catalytic and thermal pyrolysis of DS. It can be seen from Table 4 that there is a difference in the amount of compounds present in each BO, for example, acids content in the BO produced by the catalytic thermal pyrolysis of DS was below that found in the BO originated by thermal pyrolysis. The opposite was seen with the content of esters. The decrement of the acids content in the BO produced by the catalytic process compared to that produced by thermal pyrolysis process belongs to the decarboxylation reactions of the acids. Compared to the other sample, this reaction increased the alkane content in the BO produced by the catalytic thermal pyrolysis process. The increment of the esters content of the BO originated via the catalytic process may be

Table 2. Compounds identified by GC-MS for BO produced by thermal pyrolysis of DS

Compound	Chemical formula	M. Wt.	Area (%)
Benzene	C_6H_6	78	% 0.20
Furan, 2-ethyl-	C_6H_8O	88	% 0.73
Furan, 2,5-dimethyl-	C_6H_8O	88	% 1.95
Benzene, methyl- (CAS)	C_7H_8	92	% 2.08
2-Octene	C_8H_{16}	112	% 0.33
2-Ethyl-5-methylfuran	$C_7H_{10}O$	102	% 1.18
1H-Pyrazole, 1,3,5-trimethyl-	$C_6H_{10}N$	89	% 0.22
2-Vinyl-5-methylfuran	C_7H_8O	100	% 0.21
2-furan-carboxaldehyde	$C_5H_4O_2$	80	% 1.64
2-Furanmethanol	$C_5H_6O_2$	82	% 1.10
Ethylbenzene	C_8H_{10}	106	% 0.86
p-Xylene	C_8H_{10}	106	% 0.79
(Bicyclo[2.2.1]hept-1'-yl)-carbaldehyde	$C_9H_{14}O$	118	% 0.34
1-Nonene	C_9H_{18}	126	% 0.37
o-Xylene	C_8H_{10}	106	% 0.92
Nonane	C_9H_{20}	128	% 0.73
2-Cyclopenten-1-one, 2-methyl-	C_6H_8O	88	% 0.56
Ethanone, 1-(2-furanyl)-	$C_6H_6O_2$	94	% 0.65
Benzene, propyl-	C_9H_{12}	120	% 0.49
3-Hexanone	$C_6H_{12}O$	92	% 0.65
2-Furancarboxaldehyde, 5-methyl-	$C_6H_6O_2$	94	% 2.39
5 METHYL FURFURAL	$C_6H_6O_2$	94	% 0.55
Benzene, 1-ethyl-2-methyl-	C_9H_{12}	120	% 0.23
1-Decene	$C_{10}H_{20}$	140	% 0.66
Decane	$C_{10}H_{22}$	142	% 2.14
4-Decene	$C_{10}H_{20}$	140	% 0.24
2-Cyclopenten-1-one, 2-hydroxy-3-methyl	C_6H_8O	88	% 0.67
2-Cyclopenten-1-one, 2,3-dimethyl-	$C_7H_{10}O$	102	% 0.80
Benzene, n-butyl-	$C_{10}H_{14}$	134	% 0.77
Phenol, 2-methyl-	C_7H_8O	100	% 0.73
1-Undecene	$C_{11}H_{22}$	154	% 1.94
Undecane	$C_{11}H_{24}$	156	% 2.94
5-Undecene	$C_{11}H_{22}$	154	% 0.45
Benzofuran, 2-methyl-	C_9H_8O	124	% 0.60
Benzene, pentyl-	$C_{11}H_{16}$	148	% 1.39
Benzene, 1-methyl-4-butyl	$C_{11}H_{16}$	148	% 0.43
Furan, 2-(2-furanylmethyl)-5-methyl	$C_{10}H_{10}O_2$	146	% 0.43
Phenol, 2,3-dimethyl-	$C_8H_{10}O$	114	% 1.04
1-Dodecene	$C_{12}H_{24}$	168	% 1.46
Dodecane	$C_{12}H_{26}$	170	% 0.69
Benzofuran, 4,7-dimethyl-	$C_{10}H_{10}O$	138	% 0.40
Benzene, hexyl-	$C_{12}H_{18}$	162	% 0.60
Benzene, (1,3-dimethylbutyl)-	$C_{12}H_{18}$	162	% 0.38
Furan, 2,2'-methylenebis[5-methyl-	$C_{10}H_{10}O_2$	146	% 0.56
1-Tridecene	$C_{13}H_{26}$	182	% 0.48
Tridecane	$C_{13}H_{28}$	184	% 2.05
Benzene, heptyl-	$C_{13}H_{20}$	176	% 0.29
1-Tetradecene	$C_{14}H_{28}$	196	% 0.38

Table 2. Cont. Compounds identified by GC-MS for BO produced by thermal pyrolysis of DS

Tetradecane	$C_{14}H_{30}$	198	% 0.55
Benzene, octyl-	$C_{14}H_{22}$	190	% 0.31
1-Pentadecene	$C_{15}H_{30}$	210	% 0.53
2-Tridecanone	$C_{13}H_{26}O$	190	% 0.28
pentadecane	$C_{15}H_{32}$	212	% 1.88
Dodecanoic acid	$C_{12}H_{24}O_2$	184	% 12.78
7-Hexadecene, (Z)-	$C_{16}H_{32}$	224	% 0.91
1-Hexadecene	$C_{16}H_{32}$	224	% 0.46
Hexadecane	$C_{16}H_{34}$	226	% 0.79
8-Heptadecene	$C_{17}H_{34}$	238	% 3.71
8-Heptadecene	$C_{17}H_{34}$	238	% 2.51
Heptadecane	$C_{17}H_{36}$	240	% 1.57
Tetradecanoic acid	$C_{14}H_{28}O_2$	212	% 6.31
(4-Methylphenyl) methanol, 3-methylbutyl ether	$C_{13}H_{20}O$	184	% 0.62
4-Dibenzofuranamine	$C_{12}H_9NO$	168	% 0.50
7-Tridecanone	$C_{13}H_{26}O$	190	% 0.94
Glycidyl palmitate	$C_{19}H_{36}O_3$	288	% 1.29
Hexadecanenitrile	$C_{16}H_{31}N$	230	% 0.59
Hexadecanoic acid, methyl ester	$C_{17}H_{34}O$	246	% 0.30
n-Hexadecanoic acid	$C_{16}H_{32}O$	232	% 6.98
Myristic acid, 3,4-dichlorophenyl ester	$C_{20}H_{30}Cl_2O$	312	% 0.36
Allyl Cyclohexyl carbonate	$C_{10}H_{16}O_3$	160	% 1.21
Cyclopentadecanone, 2-hydroxy-	$C_{15}H_{28}O$	216	% 0.39
2-(Methyl-D3)-Cyclohexanone	$C_{13}H_{24}O$	188	% 0.85
9-Octadecenoic acid, methyl ester, (E)-	$C_{19}H_{36}O_2$	280	% 0.68
14-.BETA.-H-PREGNA	$C_{21}H_{36}$	288	% 0.71
9-Octadecenoic acid, (E)-	$C_{18}H_{34}O_2$	266	% 5.72
Oleic Acid	$C_{18}H_{34}O_2$	266	% 3.81
Octadecanoic acid	$C_{18}H_{36}O_2$	268	% 0.80

Table 3. Compounds identified by GC-MS for BO produced by catalytic pyrolysis of DS

Compound	Chemical formula	M. Wt.	Area (%)
Heptane	C_7H_{16}	100	% 1.41
Furan, 2,5-dimethyl-	C_6H_8O	88	% 3.56
Benzene, methyl- (CAS)	C_7H_8	92	% 3.59
2-Octene	C_8H_{16}	112	% 0.89
(3E,5E)-Hepta-3,5-dien-2-one	$C_7H_{10}O$	100	% 2.10
1H-Pyrazole, 3,5-dimethyl-	$C_5H_8N_2$	82	% 2.13
Benzene, ethyl-	C_8H_{10}	106	% 1.42
o-Xylene	C_8H_{10}	106	% 1.17
p-Xylene	C_8H_{10}	106	% 1.52
Nonane	C_9H_{20}	128	% 1.33
2-Furancarboxaldehyde, 5-methyl-	$C_6H_6O_2$	84	% 2.37
1-Decene	$C_{10}H_{20}$	140	% 1.02
Decane	$C_{10}H_{22}$	142	% 3.29
1-Undecene	$C_{11}H_{22}$	154	% 3.56
Undecane	$C_{11}H_{24}$	156	% 4.22
Benzofuran, 2-methyl-	C_9H_8O	114	% 0.76
Benzene, pentyl-	$C_{11}H_{16}$	148	% 1.98

Table 3. Cont. Compounds identified by GC-MS for BO produced by catalytic pyrolysis of DS

Dodecane	C ₁₂ H ₂₆	170	% 1.13
Tridecane	C ₁₃ H ₂₈	184	% 3.10
Tetradecane	C ₁₄ H ₃₀	198	% 0.94
Pentadecane	C ₁₅ H ₃₂	212	% 2.88
Dodecanoic acid	C ₁₂ H ₂₄ O ₂	184	% 16.62
8-Heptadecene	C ₁₇ H ₃₄	238	% 4.81
8-Heptadecene	C ₁₇ H ₃₄	238	% 3.38
Heptadecane	C ₁₇ H ₃₆	240	% 2.21
Tetradecanoic acid	C ₁₄ H ₂₈ O ₂	212	% 6.87
Tetrapentacontane, 1,54-dibromo-	C ₅₄ H ₁₀₈ Br ₂	826	% 1.13
Glycidyl palmitate	C ₁₉ H ₃₆ O ₃	288	% 1.55
n-Hexadecanoic acid	C ₁₆ H ₃₂ O ₂	240	% 4.68
Eicosane, 2-methyl-	C ₂₁ H ₄₄	296	% 1.27
9-Octadecenoic acid, methyl ester, (E)-	C ₁₉ H ₃₆ O ₂	280	% 1.27
9-Octadecenoic acid, methyl ester, (E)-	C ₁₉ H ₃₆ O ₂	280	% 2.11
9-Octadecenoic acid, (E)-	C ₁₈ H ₃₄ O ₂	266	% 4.88
Oleic Acid	C ₁₈ H ₃₄ O ₂	266	% 4.85

Table 4. Percentage of type of compounds for BO produced via two types of pyrolysis processes

Compound type	BO produced by catalytic pyrolysis	BO produced by thermal pyrolysis
Acids	37.90	38.79
Alkenes	25.37	31.12
n-paraffines	20.51	14.64
Aromatics	10.44	10.62
Phenols	0.0	1.77
Esters	3.38	1.34
Alcohols	0.0	1.10
Ethers	0.0	0.62
Iso-paraffines	2.4	0.0

due to the esterification reactions of the acids. On the other hand, the content of alkenes in the BO produced by the catalytic process was below that produced by the thermal pyrolysis process, and the cause could be the hydrogenation reaction of the produced alkenes by the H₂ gas produced as a non-condensable gas during the process. The iso-paraffines present in the BO originating through the catalytic process were greater than that produced via the thermal pyrolysis process, and the cause could be attributed to the presence of a catalyst, which may accelerate the isomerization reactions. The BO originating from the thermal pyrolysis process contained phenols, alcohols, and ethers. On the other side, these compounds were not present in the BO sample produced by catalytic process may be due to the dehydrogenation and dehydration reaction occurred during the catalytic pyrolysis of the feed. Types of the

organic compounds present in the attained BO samples were similar to those established for other BO samples in the literature (Mishra and Mohanty, 2020; Aljeradat et al., 2022).

¹H NMR studies

The BO samples originated by thermal catalytic and thermal pyrolysis of DS were also analyzed by ¹H spectroscopy, and their spectra are presented in Figures 5 and 6.

The ¹H NMR spectrum provides comprehensive information regarding aromatic, alkenes, and aliphatic compounds in the BO (Sut et al., 2016). Aliphatic resonances have a chemical shift of 0.5–3.0 ppm, while alkene resonance has a chemical shift of 4.5–6.3 ppm. The aromatic resonance has a chemical shift of 6.0–9.0 ppm. BO developed from the DS via thermal and catalytic pyrolysis

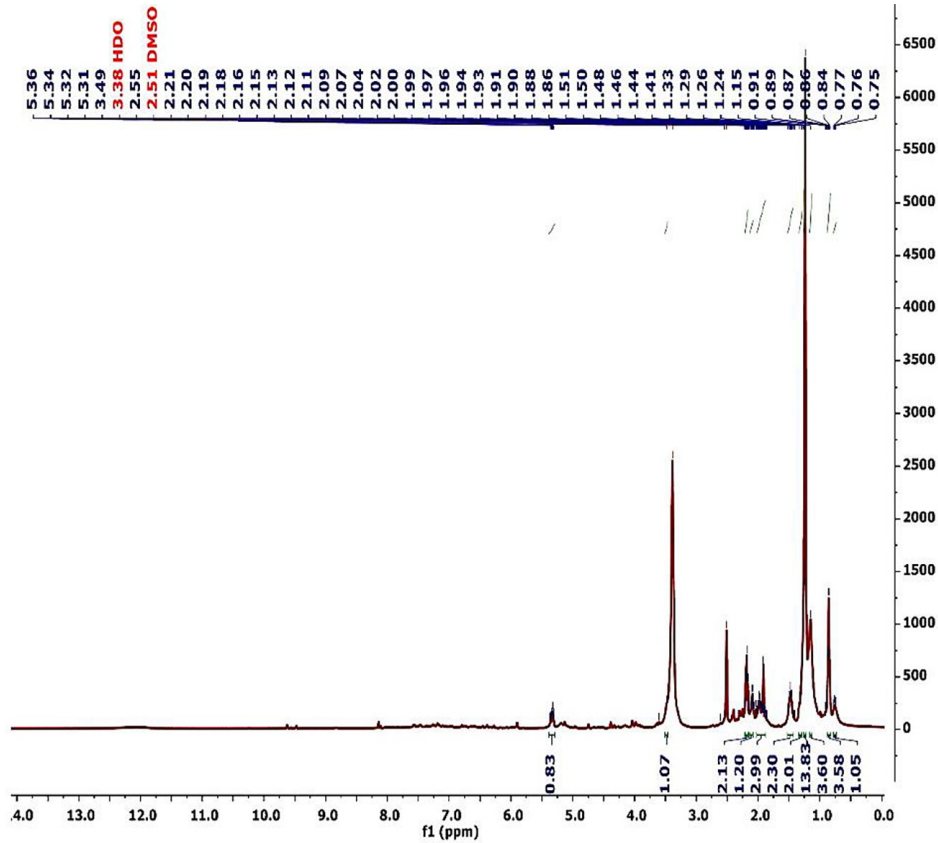


Figure 5. ¹H NMR Spectrum for BO produced by thermal pyrolysis of DS

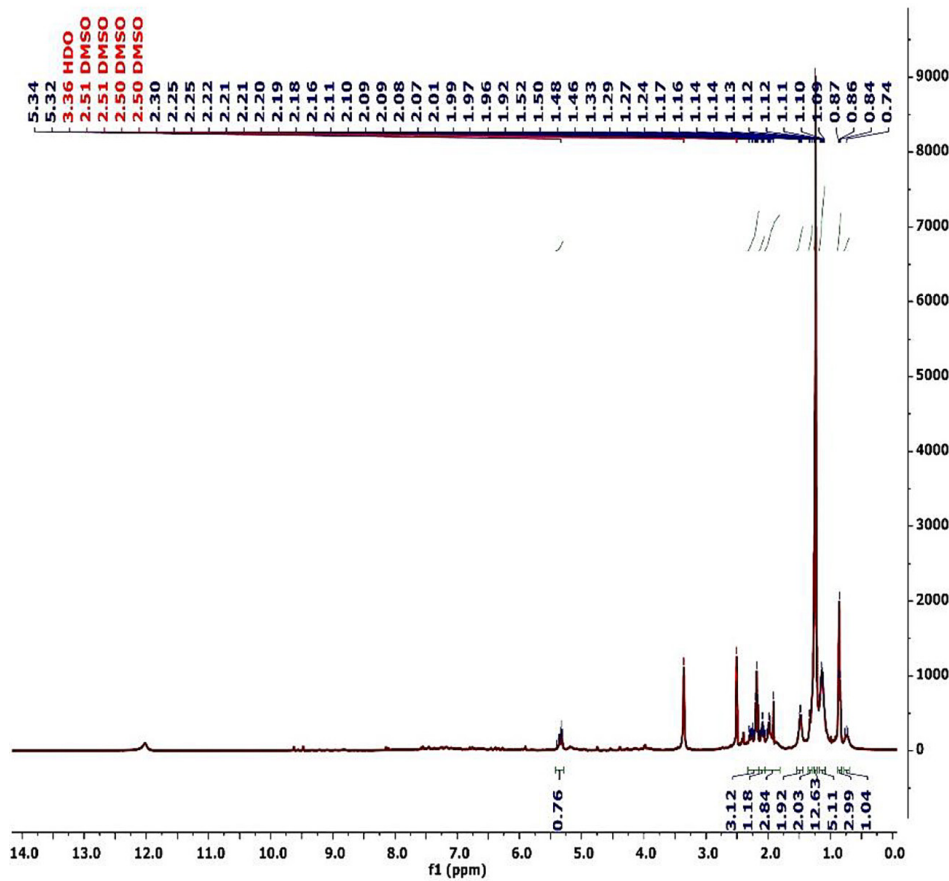


Figure 6. ¹H NMR Spectrum for BO produced by catalytic pyrolysis of DS

processes had no aromatic protons. Results from the ^1H NMR analysis disclosed that the total hydrogens in the BO originated from the DS via the catalytic thermal cracking was 32.86% compared to 34.59% for that produced via the thermal pyrolysis process. The initial area between 0.5 and 1.9 ppm is due to the aliphatic hydrocarbon chains (Bordoloi et al., 2015). This area amounted to 78.27% for the BO originating from the DS via the catalytic thermal cracking compared to 76.30% for the BO produced by the on-catalytic pyrolysis process. This result was compatible with that clarified by the GC-MS analysis. The area observed at the chemical shift of 1.8–3.0 ppm represents the aliphatic protons connected to C=C, either alkene or aromatic or two bonds abroad from heteroatom (Sut et al., 2016). This area was 27.57% for the BO produced by the catalytic pyrolysis of the DS compared to 24.91% for that originated from the DS by the thermal pyrolysis process. The region between 3 and 4.5 ppm relates to protons connected to amines, aliphatic alcohol, or a methylene group, which attaches two aromatic rings (Bordoloi et al., 2015). This region was absent in the BO sample produced by the catalytic pyrolysis of the DS compared to 3.09% for that originated from the DS by the thermal pyrolysis process, indicating that protons attached to heteroatoms are present in the latter. Finally, the area in the 4.5–7.0 ppm range refers to the protons bound to carbon atoms in the

phenolic (O-H) group or methoxyl, carbohydrate-type compounds, or alkenes (Sut et al., 2016). The area of this region was 2.26% for the BO sample produced by the catalytic pyrolysis of the DS compared to 2.39% for that originated from the DS by the thermal pyrolysis process. As per the above results, the differences in the percentages of the regions belonging to various types of hydrogen could be ascribed to the presence of the catalyst, which accelerates the devolatilization of the DS in the form of non-condensable gases, like CO, CO₂, etc. Results deduced from the ^1H NMR measurements were compatible with those obtained by the GC-MS analysis.

FTIR Spectroscopy of BO

The FTIR spectrum of the BO originated by the catalytic thermal decomposition of DS is demonstrated in Figure 7, which disclosed the occurrence of diverse compounds in the BO represented by the multiple absorbance bands at different wavenumbers. The broad absorption peak at 3,368 cm⁻¹ is assigned to the O–H stretching vibrations in R–O–H, R–C=O–H, H₂O, Ph–O–H, and polymeric hydroxyl compounds. (Mishra and Mohanty, 2020) The C–H stretching vibrations in alkanes (CH₂ and CH₃, asymmetric and symmetric) are designated by the absorbance peak at 2,922 cm⁻¹ and 2,853 cm⁻¹ (Fadhil and Kareem, 2021). The peak at 2,678 cm⁻¹ corresponded to the C–H and =C–H stretching vibrations,

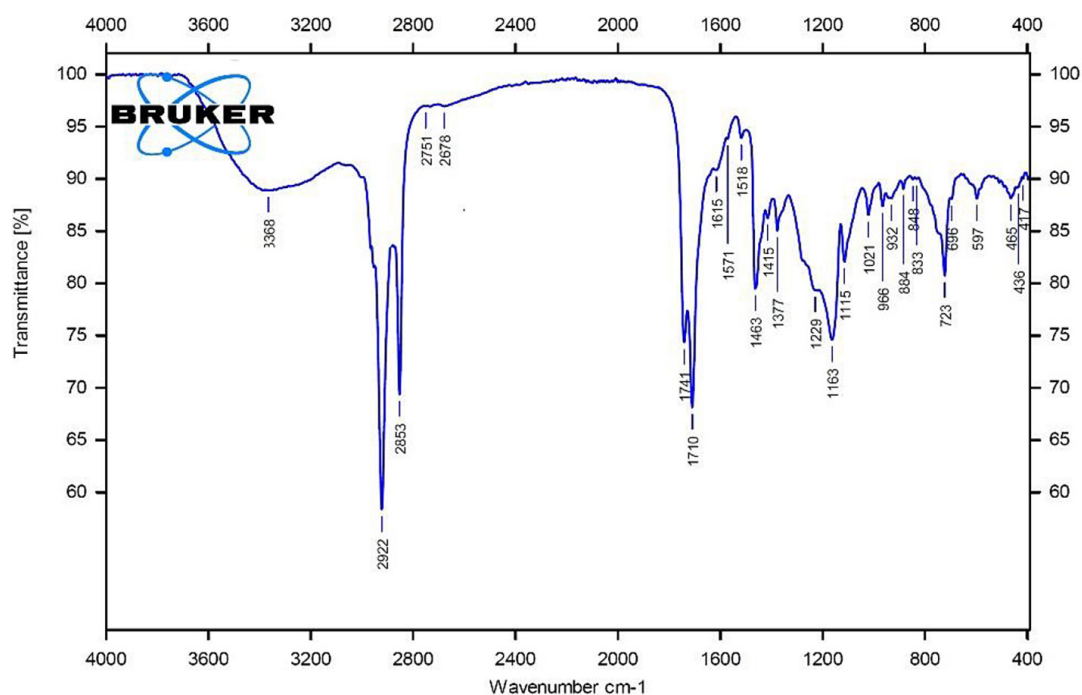


Figure 7. FTIR spectrum of the BO produced via catalytic pyrolysis of DS

demonstrating the occurrence of alkanes and alkenes (Altamer et al., 2022). The absorption peaks observed at $1,615\text{ cm}^{-1}$ and $1,710\text{ cm}^{-1}$ belong to the C=O stretching vibrations, suggesting the existence of aldehyde, ketone, and quinone groups (Mishra and Mohanty, 2018). The absorption band at $1,377\text{ cm}^{-1}$ refers to alkane groups (C–H) bending. The peak seen at $1,415\text{ cm}^{-1}$ and $1,377\text{ cm}^{-1}$ is attributed to the C–H and aliphatic C–H stretching vibrations as a result of the presence of CH_3 and phenolic compounds (Al-Layla et al., 2021). The peak at $1,021\text{ cm}^{-1}$ relates to C–O stretching vibration, signifying the occurrence of ROR and RC=O–OR (Uzun et al., 2007). The adsorption bands at 966 cm^{-1} and 696 cm^{-1} are ascribed with O–H bending vibrations, establishing the occurrence of mono and polycyclic substituted aromatics group (Mishra and Mohanty, 2020). The observed absorption bands were also announced for other BO samples from wild mustard seed (Altamer et al., 2021), *Manilkara zapota* seeds (Mishra and Mohanty, 2020), neem seed (Mishra and Mohanty, 2018), and milk thistle seeds (Al-Layla et al., 2021). Also, the functional groups identified by the FTIR spectroscopy confirmed that the BO consisted of a mixture of multiple compounds, namely hydrocarbons and oxygenated, demonstrating that the FTIR results were compatible with the results deduced from the ^1H NMR spectroscopy and GC-MS analysis.

Evolution of fuel properties of BO

The BO samples originating from the catalytic and thermal pyrolysis of DS at the typical working conditions were determined and compared with diesel fuel, as tabulated in Table 5. First, compared to diesel fuel, the color of BO was a dark black, while its odor was smoky. Table 5 demonstrated that the viscosity of the BO produced via the thermal pyrolysis process was (12.15 cSt) at $40\text{ }^\circ\text{C}$ compared to (3.07 cSt) for BO produced by the catalytic thermal pyrolysis process. This reduction in viscosity for the BO from the catalytic

thermal pyrolysis is ascribed to the presence of the catalyst, which contributed to the decrease in the O-compounds upon thermal pyrolysis of the feed. The oxygen molecules produced during pyrolysis will react with hydrogen to give considerable water. It was reported that the high viscosity of BO affects its stability and fluidity as a fuel (Mishra and Mohanty, 2020). Also, BO with a lower content of O will resist polymerization reactions, which increases the viscosity of BO with time (Mishra and Mohanty, 2018). The density of the BO from the catalytic process was below that produced via thermal pyrolysis because of the higher content of the O-compounds in the latter than the former. When the BO is planned to be utilized as a fuel, its density has to be as low as possible because this parameter impacts the fuel vaporization, atomization, fluidity, quality, and ignition and combustion features (Mishra and Mohanty, 2018). It is clear from Table 5 that the BO produced via the catalytic thermal pyrolysis had lower acidity than that produced via the thermal pyrolysis process, and the cause belongs to the reduction of the O content due to the presence of the catalyst, leading to produce a BO with a higher calorific value. It was observed that the humidity content on the BO originated by catalytic pyrolysis was much below that detected in the BO produced via the non-catalytic process may be due to the transformation of oxygen molecules into water and gases, like CO and CO_2 upon the catalytic thermal pyrolysis of DS. The presence of humidity in the BO in considerable amounts may increase the viscosity of the BO as a consequence of condensation and polymerization reactions. The BO produced by the catalytic pyrolysis had a flash point below that observed for BO produced via thermal pyrolysis, confirming that the O content in the latter was greater than that of the former. The pH of the BO relates greatly to the amount of the O-compounds present in it in particular the acidic compounds. On this account, it is obvious that the pH of the BO resulting from the catalytic pyrolysis process

Table 5. Fuel properties of BO samples produced from DS via catalytic and thermal pyrolysis

Property	BO produced via catalytic pyrolysis	BO produced via thermal pyrolysis
Density @ $15.60\text{ }^\circ\text{C}$	0.8687	0.8988
Kinematic viscosity @ $40\text{ }^\circ\text{C}$ (cSt)	3.07	12.15
Flash point ($^\circ\text{C}$)	66.0	126.0
pH	6.33	2.97
Pour point ($^\circ\text{C}$)	-5.0	2.0
Water content (wt.%)	2.50	5.0

was above that measured for the BO sample produced by the thermal pyrolysis process, confirming that the BO produced via the thermal pyrolysis had higher content of the acidic compounds than that of produced by the catalytic process. Also, the lower acidity (pH) for the BO originated by the catalytic process suggests that it possesses higher heating value than the other sample due to its lower O/C ratio.

CONCLUSIONS

The catalytic thermal pyrolysis of DS using the AKC as an effective and cheap catalyst for producing high-quality BO with properties closer to diesel fuel was successfully achieved here. The catalytic activity of the AKC was due to its surface area and mesoporous, which amounted to 119.49 m²/g and 7.13 nm, respectively. The highest yield of the pyrolytic liquid from DS via the catalytic process was 60.64 % at the typical experimental conditions of 2.5 wt.% of the AKC, 425 °C for 60 min, and 0.40 mm participle size compared to 44.0%. The pyrolytic liquid yield via the thermal pyrolysis process was 44.0% at these conditions, signifying the effectiveness of the as-prepared catalyst in the liquefaction of DS. Moreover, GC-MS analysis showed that the BO samples originating via the two processes were mainly composed of hydrocarbons, oxygenates, aromatics, and nitrogenates. However, the BO produced via the catalytic pyrolysis of DS exhibited a higher ratio of aliphatic compounds and lower content of oxygenates. Also, the fuel properties of the BO produced by the catalytic pyrolysis were superior to those measured for the BO produced by the thermal pyrolysis process, indicating the potential of the used catalyst for producing high-quality bio-oil.

Acknowledgments

Facilities provided by Mosul University, College of Science, Chemistry Department are highly appreciated by the authors.

REFERENCES

1. Agnihotri, N., Mondal, M. K. 2023. Comparison of non-catalytic and in-situ catalytic pyrolysis of *Melia azedarach* sawdust. *Journal of Analytical and Applied Pyrolysis*, 172, 106006.
2. Ahmad, M.S., Mehmood, M.A., Al Ayed, O.S., Ye, G., Luo, H., Ibrahim, M., Qadir, G. 2017. Kinetic

- analyses and pyrolytic behavior of Para grass (*Urochloa mutica*) for its bioenergy potential. *Biore-source technology*, 224, 708–713.
3. Ahmed, M.J., Theydan, S.K. 2015. Adsorptive removal of p-nitrophenol on microporous activated carbon by FeCl₃ activation: equilibrium and kinetics studies. *Desalination and Water Treatment*, 55(2), 522–531.
4. Aljeradat, R.A., Aljbour, S.H., Jarrah, N.A. 2022. Pyrolysis of date kernels using natural Jordanian Tripoli as a catalyst under different operational conditions. *Case Studies in Chemical and Environmental Engineering*, 6, 100212.
5. Al-Layla, N.M., Saleh, L.A., Fadhil, A.B. 2021. Liquid bio-fuels and carbon adsorbents production via pyrolysis of non-edible feedstock. *Journal of Analytical and Applied Pyrolysis*, 156, 105088.
6. Altamer, D.H., Al-Irhayim, A.N., Saeed, L.I. 2021. Bio-based liquids and solids from sustainable feedstock: production and analysis. *Journal of Analytical and Applied Pyrolysis*, 157, 105224.
7. Altamer, D.H., Alqazzaz, W.A., Fadhil, A.B. 2022. Adsorption behavior of rifampicin from aqueous solution onto locally available mud: Equilibrium, kinetics, and thermodynamic study. *Iranian Journal of Chemistry and Chemical Engineering*, 139–154.
8. Arabiourrutia, M., Bensidhom, G., Bolaños, M., Trabelsi, A.B.H., Olazar, M. 2022. Catalytic pyrolysis of date palm seeds on HZSM-5 and dolomite in a pyroprobe reactor in line with GC/MS. *Biomass Conversion and Biorefinery*, 1–20.
9. Bordoloi, N., Narzari, R., Chutia, R.S., Bhaskar, T., Kakti, R. 2015. Pyrolysis of *Mesua ferrea* and *Pongamia glabra* seed cover: characterization of bio-oil and its sub-fractions. *Bioresource Technology*, 178, 83–89.
10. Doshi, P., Srivastava, G., Pathak, G., Dikshit, M. 2014. Physicochemical and thermal characterization of nonedible oilseed residual waste as sustainable solid biofuel. *Waste management*, 34(10), 1836–1846.
11. Fadhil, A.B. 2021. Production and characterization of liquid biofuels from locally available nonedible feedstocks. *Asia-Pacific Journal of Chemical Engineering*, 16(1), e2572.
12. Fadhil, A.B., Alhayali, M.A., Saeed, L.I. 2017. Date (*Phoenix dactylifera* L.) palm stones as a potential new feedstock for liquid bio-fuels production. *Fuel*, 210, 165–176.
13. Fadhil, A.B., Kareem, B.A. 2021. Co-pyrolysis of mixed date pits and olive stones: Identification of bio-oil and the production of activated carbon from bio-char. *Journal of Analytical and Applied Pyrolysis*, 158, 105249.
14. Hai, A., Bharath, G., Ali, I., Daud, M., Othman, I., Rambabu, K., Banat, F. 2022. Pyrolysis of date seeds loaded with layered double hydroxide: kinetics, thermodynamics, and pyrolytic gas properties. *Energy Conversion and Management*, 252, 115127.

15. Hou, Y., Bai, Z., Lu, H., Feng, Z., Zhang, T., Jia, Y., Li, W. 2023. In-situ catalytic upgrading of Hami coal pyrolysis volatiles over acid-modified kaolin. *Fuel*, 331, 125660.
16. Hu, Z., Zheng, Y., Yan, F., Xiao, B., Liu, S. 2013. Bio-oil production through pyrolysis of blue-green algae blooms (BGAB): Product distribution and bio-oil characterization. *Energy*, 52, 119–125.
17. Li, Y., Hu, B., Fu, H., Zhang, Z.X., Guo, Z.T., Zhou, G.Z., Lu, Q. 2022. Fast pyrolysis of bagasse catalyzed by mixed alkaline-earth metal oxides for the selective production of 4-vinylphenol. *Journal of Analytical and Applied Pyrolysis*, 164, 105531.
18. Luo, W., Hu, Q., Fan, Z. Y., Wan, J., He, Q., Huang, S. X., Zhou, Z. 2020. The effect of different particle sizes and HCl-modified kaolin on catalytic pyrolysis characteristics of reworked polypropylene plastics. *Energy*, 213, 119080.
19. Mariscal, R., Maireles-Torres, P., Ojeda, M., Sádaba, I., Granados, M.L. 2016. Furfural: a renewable and versatile platform molecule for the synthesis of chemicals and fuels. *Energy & environmental science*, 9(4), 1144–1189.
20. Mekhilef, S., Saidur, R., Kamalifarvestani, M. 2012. Effect of dust, humidity and air velocity on efficiency of photovoltaic cells. *Renewable and sustainable energy reviews*, 16(5), 2920–2925.
21. Mishra, R.K., Mohanty, K. 2018. Thermocatalytic conversion of non-edible Neem seeds towards clean fuel and chemicals. *Journal of analytical and applied pyrolysis*, 134, 83–92.
22. Mishra, R.K., Mohanty, K. 2019. Thermal and catalytic pyrolysis of pine sawdust (*Pinus ponderosa*) and Gulmohar seed (*Delonix regia*) towards production of fuel and chemicals. *Materials Science for Energy Technologies*, 2(2), 139–149.
23. Mishra, R.K., Mohanty, K. 2020. Pyrolysis of Manilkara zapota seeds over ZSM-5 to produce high-quality bio-oil and chemicals. *Fuel*, 280, 118594.
24. Mohan, I., Arya, A., Singh, R., Kumar, S. 2023. Pyrolysis of Phoenix *Dactylifera* and *Phyllanthus Emblica* seeds to produce biofuel. *Materials Today: Proceedings*, 72, 713–718.
25. Paenpong, C., Pattiya, A. 2016. Effect of pyrolysis and moving-bed granular filter temperatures on the yield and properties of bio-oil from fast pyrolysis of biomass. *Journal of Analytical and Applied Pyrolysis*, 119, 40–51.
26. Pan, Y., Sima, J., Wang, X., Zhou, Y., Huang, Q. 2021. BTEX recovery from waste rubbers by catalytic pyrolysis over Zn loaded tire derived char. *Waste Management*, 131, 214–225.
27. Panda, A.K., Mishra, B.G., Mishra, D.K., Singh, R.K. 2010. Effect of sulphuric acid treatment on the physico-chemical characteristics of kaolin clay. *Colloids and surfaces A: Physicochemical and engineering aspects*, 363(1–3), 98–104.
28. Rajpoot, L., Tagade, A., Deshpande, G., Verma, K., Geed, S.R., Patle, D.S., Sawarkar, A.N. 2022. An overview of pyrolysis of de-oiled cakes for the production of biochar, bio-oil, and pyro-gas: Current status, challenges, and future perspective. *Bioresource Technology Reports*, 101205.
29. Rowhani, A., Rainey, T.J. 2016. Scrap tyre management pathways and their use as a fuel—a review. *Energies*, 9(11), 888.
30. Saidi, M., Rahimpour, H.R., Rahzani, B., Rostami, P., Gates, B.C., Rahimpour, M.R. 2016. Hydroprocessing of 4-methylanisole as a representative of lignin-derived bio-oils catalyzed by sulphided CoMo/ γ -Al₂O₃: a semi-quantitative reaction network. *The Canadian Journal of Chemical Engineering*, 94(8), 1524–1532.
31. Saidi, M., Rahzani, B., Rahimpour, M.R. 2017. Characterization and catalytic properties of molybdenum supported on nano gamma Al₂O₃ for upgrading of anisole model compound. *Chemical Engineering Journal*, 319, 143–154.
32. Silvestre, W.P., Pauletti, G.F., Baldasso, C. 2020. Fodder radish (*Raphanus sativus* L.) seed cake as a feedstock for pyrolysis. *Industrial Crops and Products*, 154, 112689.
33. Sut, D., Chutia, R.S., Bordoloi, N., Narzari, R., Katakati, R. 2016. Complete utilization of non-edible oil seeds of *Cascabela thevetia* through a cascade of approaches for biofuel and by-products. *Bioresource Technology*, 213, 111–120.
34. Toro-Trochez, J.L., Del Río, D.A.D.H., Sandoval-Rangel, L., Bustos-Martínez, D., García-Mateos, F.J., Ruiz-Rosas, R., Carrillo-Pedraza, E. S. 2022. Catalytic fast pyrolysis of soybean hulls: Focus on the products. *Journal of Analytical and Applied Pyrolysis*, 163, 105492.
35. Tursi, A. 2019. A review on biomass: importance, chemistry, classification, and conversion. *Biofuel Research Journal*, 6(2), 962–979.
36. Uzun, B.B., Pütün, A.E., Pütün, E. 2007. Rapid pyrolysis of olive residue. 1. Effect of heat and mass transfer limitations on product yields and bio-oil compositions. *Energy & fuels*, 21(3), 1768–1776.
37. Wang, B., Fu, Y., Zheng, H., Zeng, D., Xiao, R. 2021. Catalytic and noncatalytic fast pyrolysis of waste tires to produce high-value monocyclic aromatic hydrocarbons. *Journal of Analytical and Applied Pyrolysis*, 156, 105131.
38. Wang, F., Gao, N., Magdziarz, A., Quan, C. 2022. Co-pyrolysis of biomass and waste tires under high-pressure two-stage fixed bed reactor. *Bioresource Technology*, 344, 126306.
39. Younis, S.A., Mahmood, S.F., Ibraheem, S.Y., Fadhil, A.B. 2022. Preparation, characterization, and desulfurization performance of the activated carbon prepared from mixed agro-wastes: an isothermal and kinetic study. *International Journal of Environmental Analytical Chemistry*, 1–26.